Effects of disorder in FeSe: an *ab initio* study

Effects of disorder in FeSe: an *ab initio* study

Prabhakar P Singh

Department of Physics, Indian Institute of Technology Bombay, Powai, Mumbai 400076, India

E-mail: ppsingh@phy.iitb.ac.in

Abstract
Using the coherent-potential approximation, we have studied the effects of excess Fe, Se deficiency and substitutions of S and Te on the Se sub-lattice and Co, Ni and Cu on the Fe sub-lattice in FeSe. Our results show that (i) a small amount of excess Fe substantially disorders the Fe-derived bands while an Se deficiency affects mainly the Se-derived bands, (ii) the substitution of S or Te enhances the possibility of Fermi surface nesting, especially in $FeSe_{0.5}Te_{0.5}$, in spite of disordering the Se-derived bands and (iii) the electron doping through Co, Ni or Cu disorders the system and pushes down the Fe-derived bands, thereby destroying the possibility of Fermi surface nesting. A comparison of these results with the rigid-band, virtual-crystal and supercell approximations reveals the importance of describing disorder with the coherent-potential approximation.

(Some figures in this article are in colour only in the electronic version)

1. Introduction

The superconductivity in iron pnictides [1, 2] and chalcogenides [3], with the interactions resulting from charge and spin degrees of freedom of electrons delicately balanced [4–6], provides a unique opportunity to unravel the mystery of unconventional superconductivity [7–10]. From the experimental characterizations [11] of the superconducting state of the iron pnictides and chalcogenides as well as theoretical calculations [12], it seems clear that the superconductivity in these alloys is not mediated by the phonons [13]. Therefore, attempts are being made to understand the superconductivity in iron pnictides and chalcogenides in terms of spin fluctuations and related theories [14].

In spin-fluctuation theories [9, 10, 14], in addition to the proximity of the system to a magnetic instability, its Fermi surface (FS) and, in particular, the FS nesting plays a crucial role in enhancing the magnetic interactions. In turn, by tuning the magnetic properties and the FS of the system by chemical substitutions, or electron or hole doping, one can bring out the details of the superconducting properties of the system and thereby close in on the exact nature of the interaction responsible for superconductivity. Out of all the recently discovered superconducting iron pnictides and chalcogenides, FeSe and its alloys with one of the simplest crystal structures are well suited for such a study.

In FeSe, the superconducting transition temperature T_c of $\simeq 8$ K [3] increases up to 15 K with S and Te substitutions [15] but decreases rapidly with electron doping using Co, Ni or Cu substitutions [15–17]. The presence of excess Fe as well as the Se deficiency in FeSe is known to affect its superconducting properties [18]. In addition, with an increase in pressure up to 8.9 GPa, the T_c of FeSe increases to 36.7 K [19–21].

Previous theoretical attempts [22–26] at understanding the changes in the normal state electronic properties, as a prelude to understanding the changes in their superconducting properties, of several of the pnictides and chalcogenides upon alloying have used either the virtual-crystal or the supercell or a series of ordered alloys or parameterized model Hamiltonian approaches. The virtual-crystal and the supercell approaches are known to be quite inadequate to describe the effects of disorder in metallic alloys, especially in d-band metals [27]. In addition, an *ab initio* study of the effects of alloying in FeSe has been lacking so far.

In an attempt to understand the changes in the normal state electronic properties of FeSe upon alloying, which may, in turn, provide some understanding of the changes in its superconducting properties, we have used the Korringa–Kohn–Rostoker coherent-potential approximation method [27] in the atomic-sphere approximation (KKR-ASA CPA) [28] to carry out charge, self-consistent electronic structure calculations of FeSe and its alloys with S, Te, Co, Ni and Cu, including the

1

presence of excess Fe and the deficiency of Se. We have also carried out a detailed comparison of these results with the rigid-band, virtual-crystal and supercell approximations.

Based on our calculations, we find that (i) a small amount of excess Fe substantially disorders the Fe-derived bands near the Fermi energy (E_F) while Se deficiency affects mainly the Se-derived bands away from E_F, (ii) the substitution of S or Te on the Se sub-lattice enhances the possibility of FS nesting in spite of disordering the Se-derived bands, especially in the $FeSe_{0.5}Te_{0.5}$ alloy and (iii) the substitution of Co, Ni or Cu on the Fe sub-lattice disorders the system and pushes down the Fe-derived bands, thereby destroying the possibility of FS nesting. We also find that, for describing substitutional disorder, the coherent-potential approximation is more reliable than the rigid-band, virtual-crystal or supercell approximation.

2. Computational method

We have studied $Fe_{1+\delta}Se$ with $\delta = 0.0, 0.01, 0.03$ and 0.06, $FeSe_{1-x}$ with $x = 0.01, 0.03, 0.06, 0.12$ and 0.18, $FeSe_{1-y}Te_y$ with $y = 0.25$ and 0.5, $FeSe_{0.9}S_{0.1}$, $Fe_{0.9}Co_{0.1}Se$, $Fe_{0.9}Ni_{0.1}Se$ and $Fe_{0.91}Cu_{0.1}Se$ in the tetragonal ($P4/nmm$) crystal structure, while $Fe_{1.01}Se$ has been studied in the orthorhombic structure as well. The substitution of 10% Cu on the Fe sub-lattice in $Fe_{1.01}Se$ results in the composition $Fe_{0.91}Cu_{0.10}Se$, used in the cited experiment [17] and hence in our calculations. To reduce the errors due to the ASA, we have introduced four empty spheres in the unit cell containing two Fe and two Se atoms. The atomic as well as the empty-sphere positions in the unit cell are: Fe(3/4, 1/4, 0; 2a), Se(1/4, 1/4, z_{Se}; 2c), E1(1/4, 1/4, $z = -z_{Se}$; 2c) and E2(3/4, 1/4, 0.5; 2c), where E1 and E2 denote the two empty-sphere sub-lattices. The E1 empty-sphere layer, in the same plane as the Se layer, was used to accommodate the excess Fe in the calculations of $Fe_{1+\delta}Se$ and $Fe_{0.91}Cu_{0.1}Se$. To see the effects of incorporating the excess Fe in other interstitial regions, we have also used the E2 empty-sphere site for the excess Fe in $Fe_{1.06}Se$ and sites just below the Se plane.

To model the effects of disorder, we have used the CPA [29, 27] rather than a rigid-band, virtual-crystal or supercell method because CPA has been found to reliably describe the effects of disorder in metallic alloys [28, 27]. We used the Barth and Hedin [30] exchange–correlation potential. The Brillouin zone (BZ) integration during self-consistency was carried out using a grid of $24 \times 24 \times 20$ points in the BZ. The density of states (DOS) was calculated with a grid of $28 \times 28 \times 24$ points in the BZ except for the pure FeSe and FeTe, where a grid of $36 \times 36 \times 32$ points was used. For both DOS and spectral function calculations, we have added a small imaginary component of 1 mRyd (1.5 mRyd for FeSe and FeTe) to the energy. In the following figures the Se-derived s-band is not shown. In our calculations, the lattice parameters a and c were taken from experiments [15, 18, 16, 17] while the theoretically relaxed z values were taken from [13]. For some of the intermediate alloys, we used the concentration-weighted average of the z values. The lattice parameters of FeSe, FeTe and their alloys, used in the present calculations, are listed in table 1.

Table 1. The experimental lattice parameters a and c of FeSe, FeTe and their alloys used in the present calculations.

Alloy	a (Å)	c (Å)	Alloy	a (Å)	c (Å)
FeSe	3.765	5.518	$Fe_{0.90}Co_{0.10}Se$	3.7637	5.5043
$Fe_{1.01}Se$, $FeSe_{0.99}$	3.7734	5.5258	$Fe_{0.90}Ni_{0.10}Se$	3.7713	5.503
$Fe_{1.03}Se$, $FeSe_{0.97}$	3.7787	5.5208	$Fe_{0.91}Cu_{0.10}Se$	3.807	5.495
$Fe_{1.06}Se$, $FeSe_{0.94}$	3.7747	5.5229	$FeSe_{0.90}S_{0.10}$	3.763	5.503
$Fe_{1.125}Se$, $FeSe_{0.88}$, $FeSe_{0.875}$	3.7747 3.7693	5.5229 5.4861	$FeSe_{0.75}Te_{0.25}$ $FeSe_{0.50}Te_{0.50}$	3.7989 3.7909	5.9685 5.9570
$FeSe_{0.82}$	3.7676	5.4847	FeTe	3.8215	6.2695

We have analyzed our results using the Bloch spectral function [27] $A(\mathbf{k}, E)$, defined by

$$A(\mathbf{k}, E) = -\frac{1}{\pi} \Im G(\mathbf{k}, E), \qquad (1)$$

where $G(\mathbf{k}, E)$ is the $\mathbf{k}$-space coherent-potential Green's function, and $\mathbf{k}$ and E represent the wavevector and the energy, respectively, of the electron. The band structure along the BZ symmetry directions was calculated by evaluating equation (1) for the given $\mathbf{k}$ points and the energy E in the given range. The Fermi surface in a given $\mathbf{k}$-space plane was mapped by evaluating equation (1) over a two-dimensional grid of 151×151 $\mathbf{k}$ points in the plane at the Fermi energy $E = E_F$. The peaks in the spectral function $A(\mathbf{k}, E_F)$ form the Fermi surface of the alloy. All the plots of the band structures and the Fermi surfaces were carried out with the same value for the color map in the range of 0–30 (15 for the Fermi surface) with the minimum and maximum values represented by blue and red, and the intermediate values assigned colors varying from blue, light blue, green, yellow, orange to then red. Thus, a movement away from red and towards blue in the band structure and Fermi surface plots indicates a reduction in the peak value of $A(\mathbf{k}, E)$.

The formation energy, E_{form}, of excess Fe in $Fe_{1+\delta}Se$ and the Se vacancy in $FeSe_{1-x}$ alloys has been calculated as

$$E_{form}^e = E_{Fe_{1+\delta}Se} - E_{FeSe} - \delta E_{Fe} \qquad (2)$$

$$E_{form}^v = E_{FeSe_{1-x}} - E_{FeSe} + x E_{Se} \qquad (3)$$

where the superscripts e and v correspond to the formation energy of FeSe with excess Fe or with Se vacancy, respectively. The subscripts on the right-hand side of equations (2) and (3) denote the calculated total energies of the corresponding alloys except for E_{Fe} and E_{Se}, which represent the corresponding free atom energy.

The rigid-band calculations were carried out by first determining the amount of shift in Fermi energy required to either accommodate or remove a given number of electrons from the self-consistent potential of the ordered FeSe. The Fermi surface in the rigid-band was then evaluated by the KKR-ASA CPA method at the shifted Fermi energy and using the self-consistent potential of ordered FeSe.

For the virtual-crystal approximation [31], we replaced the disordered sub-lattice by an ordered sub-lattice containing
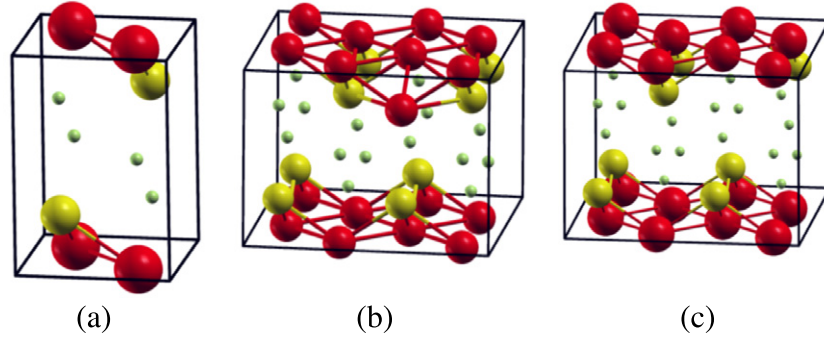
Figure 1. The unit cell of (a) tetragonal FeSe and the $2 \times 2 \times 1$ supercells used for (b) Fe_9Se_8 and (c) Fe_8Se_7 calculations. The large spheres represent Fe (red/black) and Se atoms (yellow/gray), and the smaller spheres represent empty spheres (gray). The excess Fe in Fe_9Se_8 is placed at an empty-sphere site while the vacancy in Fe_8Se_7 is formed by replacing an Se atom by an empty sphere.

a *virtual* atom, and then carried out a charge, self-consistent calculation for the alloy with the virtual atom using the KKR-ASA CPA method. The virtual atom on a sub-lattice was constructed by adding the concentration-weighted average of the valence electrons of the respective atoms on the sub-lattice to the core electrons of the atom having the higher concentration. For example, the atomic number of the virtual atom on the Fe sub-lattice in the $Fe_{0.9}Ni_{0.1}Se$ alloy is 26.2.

In the supercell approximation for excess Fe in $Fe_{1.125}Se$ and the Se vacancy in $FeSe_{0.875}$, we used a $2a \times 2a \times c$ supercell of FeSe containing 32 sites (16 atomic and 16 empty-sphere sites) as shown in figure 1. The excess Fe in Fe_9Se_8 is placed at an empty-sphere site while the vacancy in Fe_8Se_7 is formed by replacing an Se atom by an empty sphere. The charge self-consistent calculations for the supercells were carried out using the KKR-ASA CPA method. The Brillouin zone (BZ) integration during self-consistency was carried out using a grid of $12 \times 12 \times 20$ points in the BZ. The density of states (DOS) was calculated with a grid of $14 \times 14 \times 24$ points in the BZ. For DOS and spectral function calculations, we have added a small imaginary component of 2 mRyd and 1 mRyd, respectively, to the energy. We have also checked our results from the supercell calculations with the LMTO-ASA method.

3. Ordered FeSe and FeTe in the atomic-sphere approximation

To be able to separate out the effects of disorder from the atomic-sphere-approximation-related changes, in this section we compare the electronic structure of ordered FeSe and FeTe alloys with the more accurate full-potential results. In figures 2–4, we show the band structure, the density of states and the Fermi surface of FeSe and FeTe alloys, which are similar to those of [13] except for the gap between Se- and Fe-derived bands around 2.5 eV below E_F in FeSe. Since it is already known that electronic structure calculations of FeSe are very sensitive to the height of the Se layer above the Fe plane, we have carried out full-potential, linear muffin-tin orbital (FP-LMTO) calculations for FeSe using the lattice parameters as above. We find that the gap predicted by FP-LMTO is ≈ 0.3 eV, which increases to ≈ 0.4 eV if the muffin-tin spheres are enlarged to atomic spheres within the full-potential approach. In the atomic-sphere approximation, which
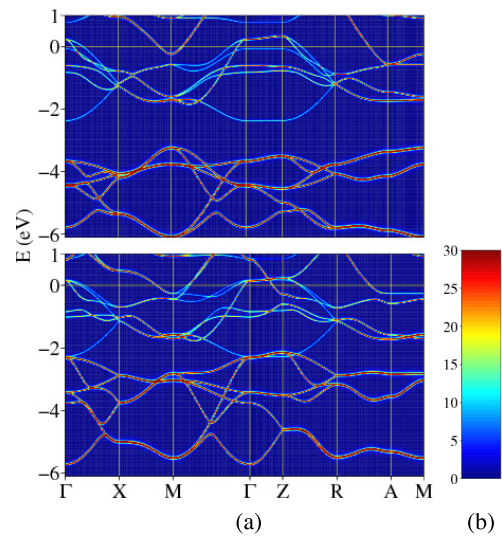

Figure 2. (a) The band structure of tetragonal FeSe (top) and FeTe (bottom) along the BZ symmetry directions using experimental lattice parameters and theoretically relaxed z_{Se}. The Fermi energy is indicated by the horizontal line at 0 eV. (b) The color map used for all the band structure and Fermi surface plots as described in the text.

uses additional approximations, including that of making the potential spherical, the gap is found to be ≈ 0.8 eV. However, the Fe-derived bands, which are responsible for superconductivity in these alloys, compare well with the more accurate FP-LMTO calculations as well as with that of [13].

Using the idea of FS nesting, it is possible to get some quantitative measure of the response of the system without evaluating the susceptibility. For example, if the FS around the Γ point matches exactly with the FS around the M point when displaced by a reciprocal space vector then the nesting is optimal. In the present context, the optimal nesting corresponds to FS at Γ and M points having matching radii and sharp Fermi surfaces (reflected by thin red lines in the figures). Any deviation, either from the matching radii or sharpness of the Fermi surfaces (reflected by diffused and/or broadened lines in the figures), generally reduces the effect of nesting.

The FS of FeSe, shown in figure 4, consists of two hole-like sheets around the Γ point and two electron-like sheets around the M point, both sheets being derived from the xz (yz) and xy bands of Fe. In FeTe, there are three hole-like sheets
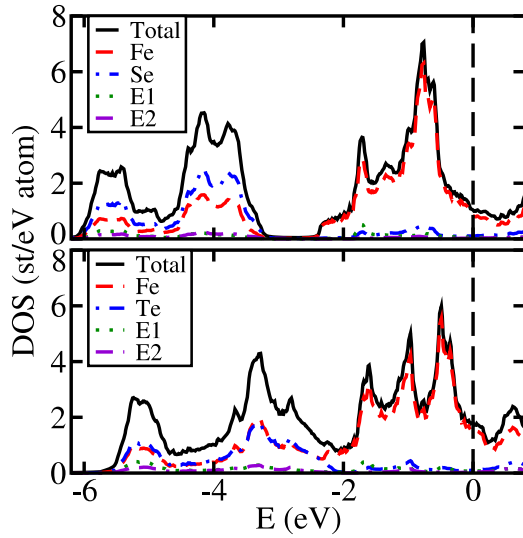
Figure 3. The total (black, solid) and the sub-lattice-resolved DOS of tetragonal FeSe (top) and FeTe (bottom) obtained using experimental lattice parameters and theoretically relaxed z_{Se}. The contributions from the Fe (red, dashed) and the Se/Te (blue, dotted–dashed) sub-lattices as well as from the empty-sphere sub-lattices E1 (green, dotted) and E2 (violet, double-dashed–dotted) are shown. The vertical, dashed line denotes the Fermi energy. Note that the total DOS in the figure corresponds to per two atoms.
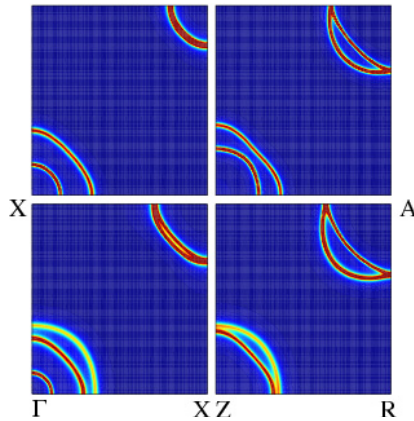

Figure 4. The Fermi surface of FeSe (top) and FeTe (bottom) in Γ–X–M and Z–R–A planes obtained using experimental lattice parameters and theoretically relaxed z_{Se}.

around the Γ point and only two sheets around the M point as shown in figure 4. The Fermi surfaces shown in figure 2 reveal enhanced FS nesting at the Γ–X–M plane in FeSe rather than in FeTe. Note that the two bands around the M point in FeSe are not resolved in figure 2. In the following, we will see if the changes in the shape and the nesting of the FS of FeSe induced upon alloying can be used to understand the changes in the superconducting properties of these alloys within the framework of the spin-fluctuation theories.

4. Effects of theoretical versus experimental z_{Se}

The role of Se height above the Fe plane, given by z_{Se}, plays a crucial role in determining the electronic properties, especially
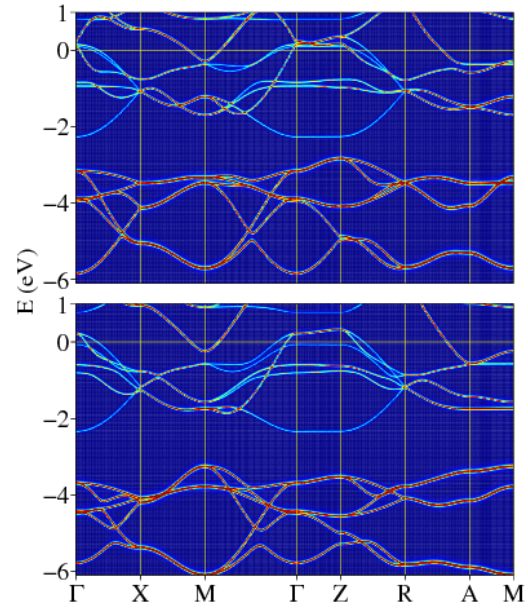

Figure 5. The band structure of tetragonal FeSe along the BZ symmetry directions using experimental lattice parameters with z_{Se} equal to its experimental (top) or theoretically relaxed (bottom) value. In both the calculations, the exchange–correlation potential was parameterized within the generalized-gradient approximation as described in the text. The Fermi energy is indicated by the horizontal line at 0 eV.
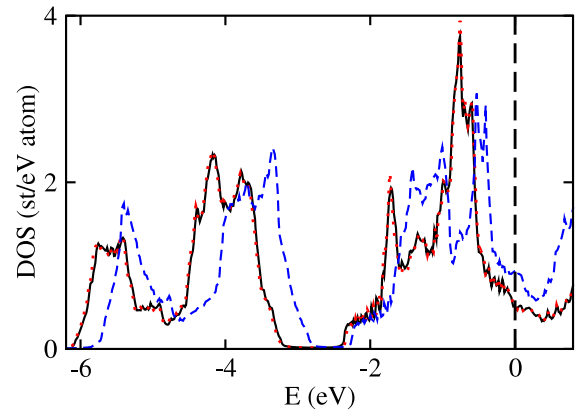

Figure 6. The total DOS of tetragonal FeSe with the experimental lattice parameters, including experimental z_{Se} (blue, dashed) and theoretical z_{Se} (red, dotted) calculated within the generalized-gradient approximation. The total DOS of FeSe (black, solid) as obtained in figure 3 is also shown.

the magnetic properties [32], of FeSe and its alloys. It is not surprising that z_{Se} plays such an important role in deciding the electronic properties of FeSe because a change in z_{Se} directly impacts the Fe d-orbitals which, in turn, affect the Fe-derived d-bands around E_F. Most of the theoretical work on FeSe has used the experimental values of the lattice parameters a and c, and the theoretically relaxed value for z_{Se}. To see what role z_{Se} plays in the present context, we have studied FeSe and its alloys using the experimental value of $z_{Se} = 0.266$ and the theoretically relaxed value of $z_{Se} = 0.2343$ [13].

In figure 5, we show the band structure of FeSe calculated with the experimental as well as the theoretically relaxed value
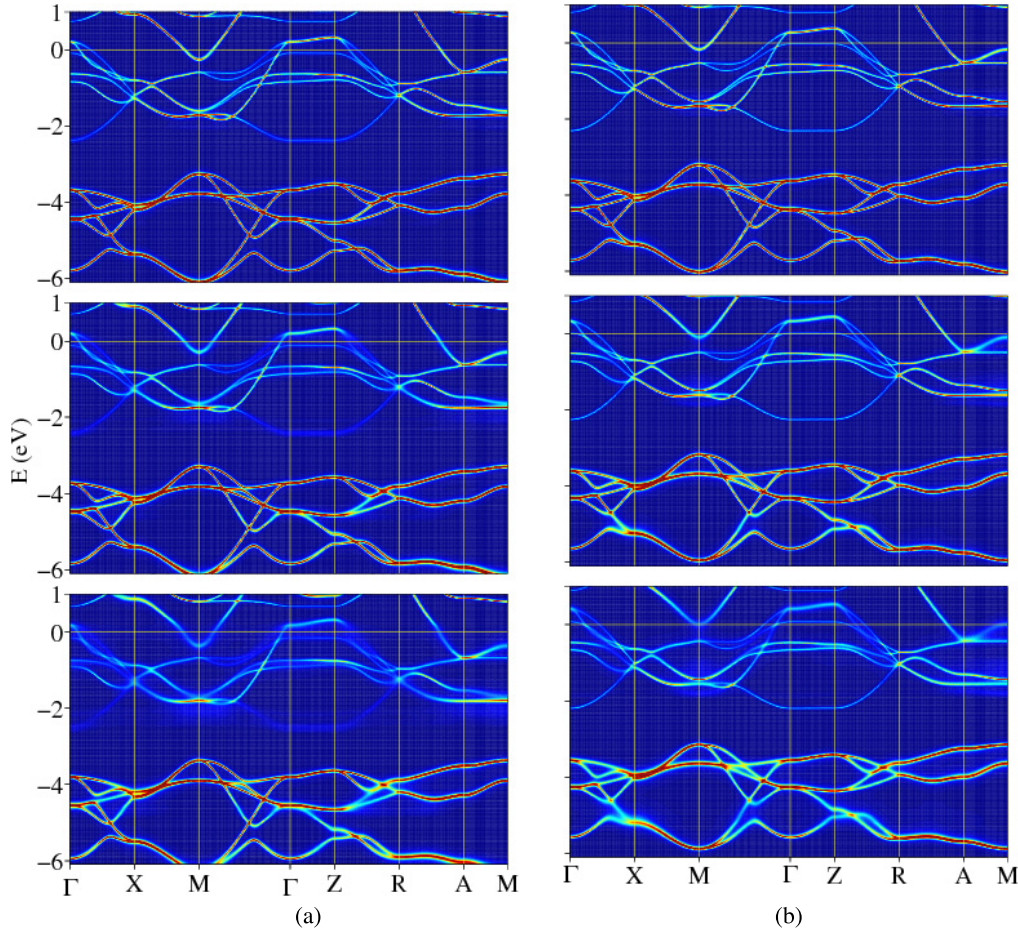
Figure 7. The band structure of (a) $Fe_{1+\delta}Se$ and (b) $FeSe_{1-x}$ with δ and $x = 0.01$ (top), 0.03 (middle) and 0.06 (bottom) along the BZ symmetry directions. The Fermi energy is indicated by the horizontal line at 0 eV.

of z_{Se}. In both cases, the experimental values of the lattice parameters a and c were used, and the exchange–correlation potential was parameterized using the generalized-gradient approximation of Perdew *et al* [33]. The use of experimental z_{Se}, which is larger than the theoretical value, allows most of the bands, including the Se-derived bands, to move up with respect to E_F. Such a movement results in three bands crossing E_F along Γ–X, M–Γ and Z–R. The use of theoretical z_{Se}, which reduces the Se height above the Fe plane, affects the individual Fe-derived d-bands around E_F differently due to the orientation of the d-orbitals. In particular, we find that the $3z^2 - 1$-derived band along Γ–X and Γ–Z is suppressed more than the other two bands, resulting in only two bands crossing E_F along Γ–X, M–Γ and Z–R for theoretically relaxed z_{Se}.

The effects of using experimental or theoretical z_{Se} get amplified in the total DOS as shown in figure 6. The higher value of z_{Se} shifts the DOS towards E_F as well as redistributes some of the electronic states between 0 and −2 eV. The Fe peak in the DOS is closer to E_F for the experimental z_{Se} than for the theoretical z_{Se}. From figure 6, we also find that the DOS of FeSe obtained with the Barth–Hedin exchange–correlation potential is essentially identical to the DOS obtained with the Perdew–Wang [34] exchange–correlation potential within the local-density approximation.

We have also calculated the Fermi surface of FeSe with experimental and theoretical z_{Se}. As discussed above, in the context of the band structure of FeSe, we find three bands around the Γ and Z points for experimental z_{Se}.

5. Electronic structure of disordered $Fe_{1+x}Se$ and $FeSe_{1-x}$ alloys

Generally, the synthesis of FeSe results in an alloy with either excess of Fe or deficiency in Se [18, 35, 17]. Measurements on such alloys have shown that $Fe_{1+\delta}Se$ is superconducting only when $\delta \leqslant 0.01$ and the underlying lattice is orthorhombic [16]. On the other hand, Se-deficient alloys $FeSe_{1-x}$ remain superconducting for $x \leqslant 0.18$ in the tetragonal structure [3, 18]. In order to understand the contrasting superconducting properties of $Fe_{1+\delta}Se$ and $FeSe_{1-x}$ alloys, we have studied their normal state electronic structure as a function of δ and x with $0 \leqslant \delta \leqslant 0.06$ and $0 \leqslant x \leqslant 0.18$.

The changes in the band structure, the density of states and the FS in $Fe_{1+\delta}Se$ and $FeSe_{1-x}$ alloys with increasing δ and x are shown in figures 7–10. In the unit cell, the excess Fe atom, denoted by Fe(2) (the Fe at the stoichiometric site is denoted by Fe(1)), is kept in the Se plane with $z_{Fe} = -z_{Se}$, which is one of the two inequivalent sub-lattices containing empty
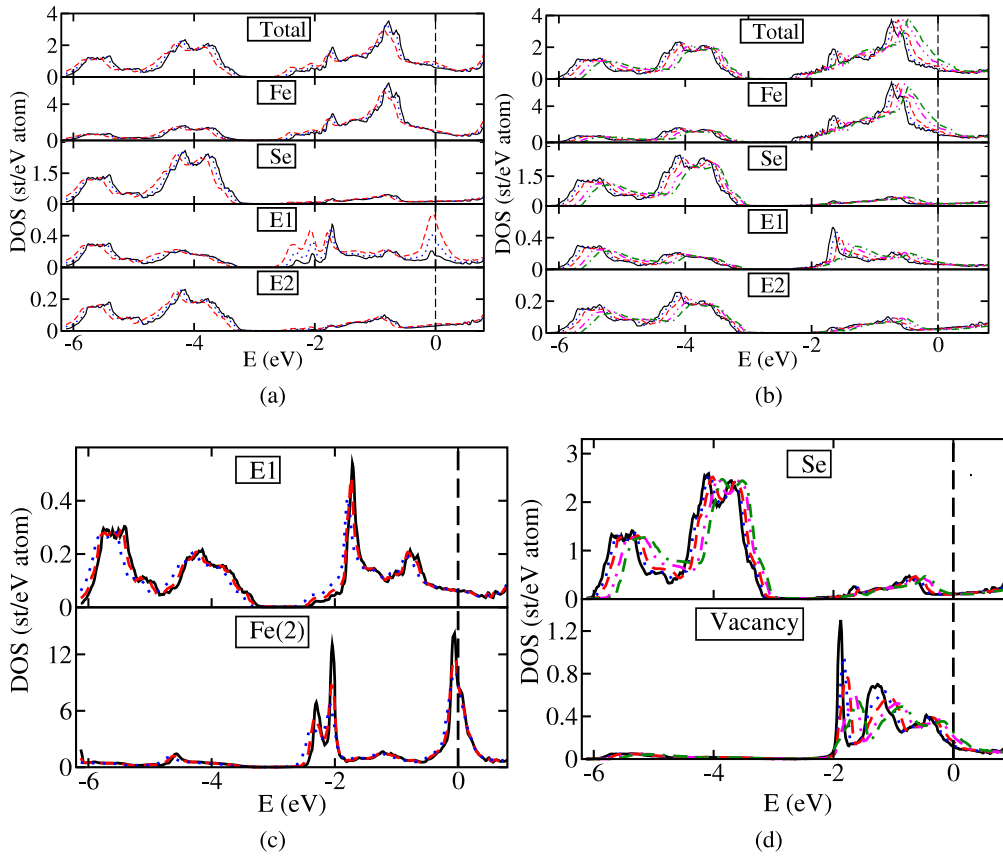
Figure 8. The total and the sub-lattice-resolved DOS of (a) $Fe_{1+\delta}Se$ and (b) $FeSe_{1-x}$ with δ and $x = 0.01$ (black, solid), 0.03 (blue, dotted) and 0.06 (red, dashed). For $FeSe_{1-x}$, the DOS corresponding to $x = 0.12$ (magenta, double-dotted–dashed) and 0.18 (green, double-dashed–dotted) are also shown. The vertical, dashed line denotes the Fermi energy. The atom-resolved DOS at (c) the E1 site of $Fe_{1+\delta}Se$ and (d) the Se site of $FeSe_{1-x}$ are also shown.

spheres. Our main conclusions are independent of the possible locations of the excess Fe atoms within the FeSe lattice, as was found in [18]. The increase in disorder induced by the presence of excess Fe can be clearly seen, as indicated by the diffused intensity, in the Fe-derived bands in figure 7(a). The Se-derived bands are left relatively untouched by the excess Fe. From the DOS of $Fe_{1+\delta}Se$ alloys, shown in figures 8(a) and (c), and 9, we find that the excess Fe kept on the E1 sub-lattice creates states around E_F and around -2 eV. The possibility of the excess Fe becoming magnetic due to the increased local density of states at E_F can be clearly seen in the d-resolved DOS of Fe(1) and Fe(2) in figure 9. On the other hand, the increase in excess Fe quickly destroys the FS nesting as seen from figure 10(a). Note that, even for $\delta = 0.01$, the nesting is not optimal.

For $Fe_{1.01}Se$ in the orthorhombic structure, the overall change in electronic structure with respect to the tetragonal structure is symmetry-induced and minimal. There are three bands crossing E_F around the Γ point instead of two bands, as is the case in the tetragonal structure, leading to some changes in the FS around the Γ point. The DOS remains essentially unchanged with respect to the tetragonal case.

The $FeSe_{1-x}$ alloys remain superconducting over a wide range of x values, indicating an unusually small impact on the bands around E_F due to vacancies in the alloy. Our results for $FeSe_{1-x}$ alloys, shown in figures 7–10, seem to
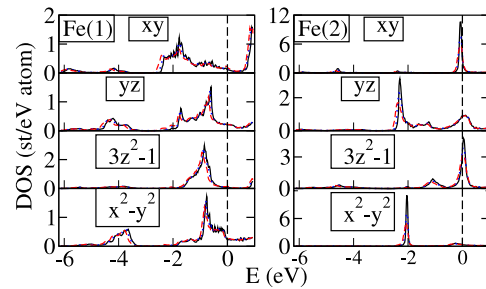

Figure 9. The d-resolved DOS at the Fe(1) (left panel) and Fe(2) (right panel) sites in $Fe_{1+\delta}Se$ with $\delta = 0.01$ (black, solid), 0.03 (blue, dotted) and 0.06 (red, dashed). The vertical, dashed line denotes the Fermi energy.

confirm it. The vacancies on the Se sub-lattice affect the Se-derived bands which are away from E_F, leaving the bands around E_F essentially untouched for small x. In addition to the lowering of E_F due to electron loss, for $x \geqslant 0.06$ the bands around E_F begin to get affected by disorder. For example, for $x \geqslant 0.12$, we find that the Se-derived bands have been substantially diffused. The loss of electrons due to increasing Se vacancy moves E_F inward, seen clearly in figure 8(b), bringing the peak in DOS due to the stoichiometric Fe closer to E_F as shown in figure 8(d), and thereby increasing
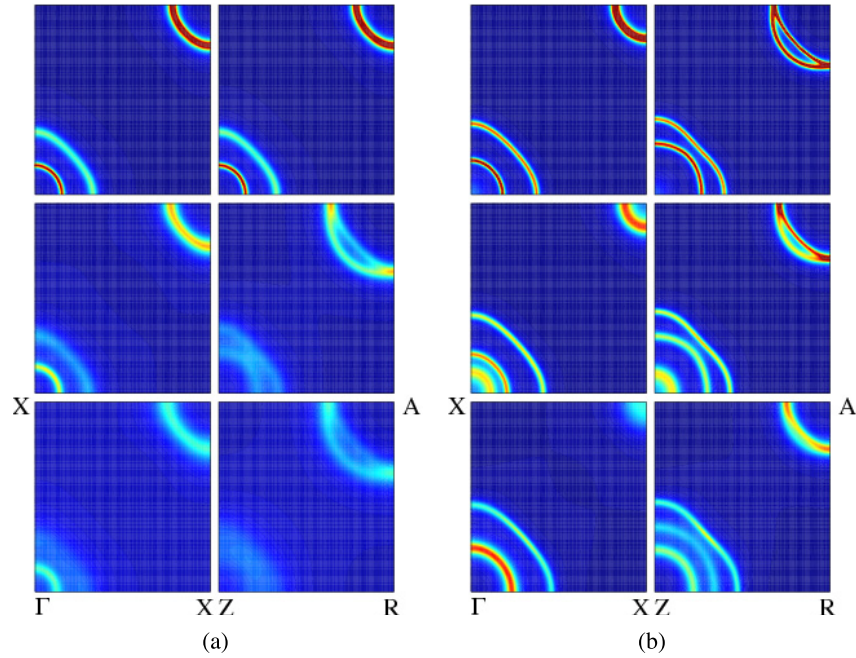
Figure 10. The Fermi surface of (a) $Fe_{1+\delta}Se$ and (b) $FeSe_{1-x}$ with δ and $x = 0.01$ (top), 0.03 (middle) and 0.06 (bottom) in Γ–X–M and Z–R–A planes.

the total DOS at E_F. The largest contribution to the DOS at E_F comes from the states of Fe(1) having $x^2 - y^2$ and xy symmetries. Such an increase in the DOS at E_F may lead to magnetism in the alloy [23]. We emphasize that Fe(2) atoms are responsible for possible magnetism in $Fe_{1+\delta}Se$, while Fe(1) atoms may lead to magnetic behavior in $FeSe_{1-x}$. With increasing x, the gradual loss of possible FS nesting in $Fe_{1+\delta}Se$ and $FeSe_{1-x}$ can also be seen in figure 10. If FS nesting is crucial for superconductivity in $FeSe_{1-x}$ alloys then clearly the possibility of superconductivity is diminished for large x as the nesting is essentially destroyed as shown in figure 10. However, experiments [35, 17] have shown that $FeSe_{1-x}$ for large x, contain impurity phases such as elemental Fe, leading to incorrect determination of Se content. Therefore, the Se content in superconducting $FeSe_{1-x}$ alloys must be determined carefully.

In both $Fe_{1+\delta}Se$ and $FeSe_{1-x}$, our results clearly show that the effects of excess Fe or Se deficiency on the electronic structure of FeSe are very different, and that for $x \geqslant 0.06$ the FS nesting is essentially destroyed.

6. Energetics of excess Fe and Se deficiency in FeSe

To get an estimate of the energetics involved in the formation of FeSe alloys with either excess Fe or Se deficiency, we have calculated the formation energy of $Fe_{1+\delta}Se$ and $FeSe_{1-x}$ alloys as described in section 2. In $Fe_{1+\delta}Se$, we find that the formation energy $E_{form}^e = -98, -94$ and -87 meV/atom for $\delta = 0.01, 0.03$ and 0.06, respectively. The vacancy formation energy in $FeSe_{1-x}$ alloys is found to be $E_{form}^v = 115, 126, 132, 134$ and 136 meV/atom for $x = 0.01, 0.03, 0.06, 0.12$ and 0.18, respectively. As our calculations are done within the atomic-sphere approximation and without taking relaxation
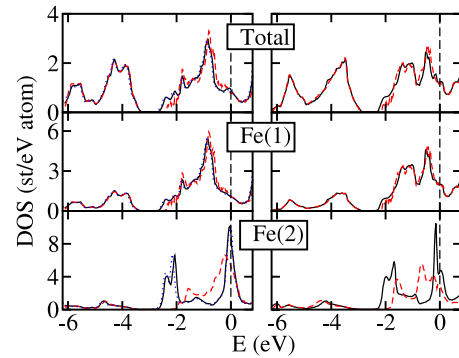

Figure 11. The total and the Fe(1) and Fe(2) DOS in $Fe_{1.06}Se$ with theoretically relaxed z_{Se} (left panel) and experimental z_{Se} (right panel). The DOS correspond to different positions of the excess Fe (Fe(2)) given by $z_{Fe} = -z_{Se}$ (black, solid) with Fe(2) in the Se plane, $z_{Fe} = 0.7755$ (blue, dotted) with Fe(2) slightly below the Se plane and $z_{Fe} = 0.5$ (red, dashed) with Fe(2) in the middle of the two Se planes. The vertical, dashed line denotes the Fermi energy.

into account, these results are expected to change with the incorporation of full-potential and relaxation effects [23].

In order to check the effects of keeping the excess Fe in $Fe_{1+\delta}Se$ at the various interstitial regions, we have studied the $Fe_{1.06}Se$ alloy keeping the excess Fe (Fe(2)) in the Se plane with $z_{Fe} = -z_{Se}$, slightly below the Se plane with $z_{Fe} = 0.7755$ and in the middle of the two Se planes with $z_{Fe} = 0.5$ for theoretically relaxed z_{Se} as well as experimental z_{Se}. As noted in section 4, the DOS of FeSe and its alloys are expected to be different for theoretically relaxed z_{Se} and experimental z_{Se}, as is the case for $Fe_{1.06}Se$ in figure 11. Not surprisingly, the DOS corresponding to $z_{Fe} = -z_{Se}$ and $z_{Fe} = 0.7755$ are essentially identical for theoretically relaxed z_{Se}.

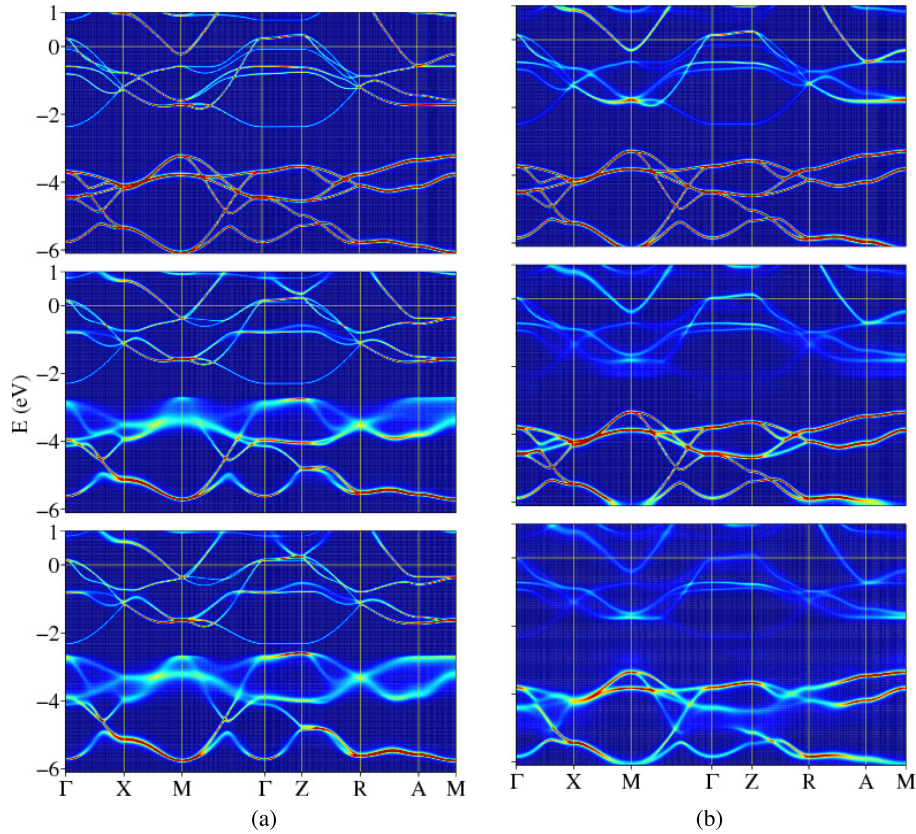**Figure 12.** The band structure of (a) $FeSe_{0.9}S_{0.1}$ (top), $FeSe_{0.75}Te_{0.25}$ (middle) and $FeSe_{0.5}Te_{0.5}$ (bottom), and (b) $Fe_{0.9}Co_{0.1}Se$ (top), $Fe_{0.9}Ni_{0.1}Se$ (middle) and $Fe_{0.91}Cu_{0.1}Se$ (bottom) along the BZ symmetry directions. The Fermi energy is indicated by the horizontal line at 0 eV.

However, when the excess Fe is placed in between the two Se planes instead of in the Se plane, the resulting Fe(2) DOS's are somewhat different from each other, as shown in the bottom panel of figure 11. These differences arise due to the relatively free space available to Fe(2) when $z_{Fe} = 0.5$. We also find that it is only with the inclusion of the Madelung potential in the muffin-tin-corrected total energy that Fe(2) prefers to go to $z_{Fe} = -z_{Se}$ instead of $z_{Fe} = 0.5$ by 11 meV/atom for experimental z_{Se}. We must point out that a more reliable way of calculating the site preference involving different structures is through the full-potential approach with relaxation included.

7. Electronic structure of disordered $FeSe_{0.9}S_{0.1}$, $FeSe_{1-y}Te_y$, $Fe_{0.9}Co_{0.1}Se$, $Fe_{0.9}Ni_{0.1}Se$ and $Fe_{0.91}Cu_{0.1}Se$ alloys

To understand the changes in the superconducting properties of FeSe upon substitution of impurities through the changes in the normal state electronic properties, we have studied the effects of substituting S and Te on the Se sub-lattice and Co, Ni and Cu on the Fe sub-lattice. In figures 12–14, we show our results for the band structure, density of states and FS of $FeSe_{0.9}S_{0.1}$, $FeSe_{0.75}Te_{0.25}$, $FeSe_{0.5}Te_{0.5}$, $Fe_{0.9}Co_{0.1}Se$, $Fe_{0.9}Ni_{0.1}Se$ and $Fe_{0.91}Cu_{0.1}Se$ alloys. Based on the atomic-size mismatch, it is expected that the substitution of Te would lead to more disorder than the substitution of S on the Se sub-lattice in FeSe. Indeed, we find that the effects of disorder are

minimal due to S but substitution of Te creates states in the gap region with substantial disorder in the Se-derived bands. The states created in the gap between Se- and Fe-derived bands can be clearly seen in figures 12(a) and (c). Surprisingly, for the $FeSe_{0.5}Te_{0.5}$ alloy, we find that the substitution of Te has rearranged the bands around E_F such that the possibility of FS nesting is maximized as shown in the bottom panel of figure 14(a).

The presence of Co, Ni and Cu in the Fe sub-lattice of FeSe is expected to affect the bands around E_F as well as move E_F up due to disorder and electron doping, thereby significantly changing its superconducting properties. As shown in figure 12(b), a 10% addition of Ni or Cu moves E_F above the two bands around the Γ point. The substitution of Cu seems to disorder both the Fe-and the Se-derived bands, as can be seen from the diffused intensity of the bands in figure 12(b). The addition of Co, Ni or Cu creates states in the gap region around -2 eV as seen from figures 13(b) and (d). The combined effect of disorder and electron addition diminishes the possibility of FS nesting in $Fe_{0.9}Co_{0.1}Se$ and destroys it in $Fe_{0.9}Ni_{0.1}Se$ and $Fe_{0.91}Cu_{0.1}Se$, as seen in figure 14(b).

8. Describing disorder: rigid-band, virtual-crystal, supercell and coherent-potential approximations

In order to emphasize the importance of describing the effects of substitutional disorder accurately and reliably in
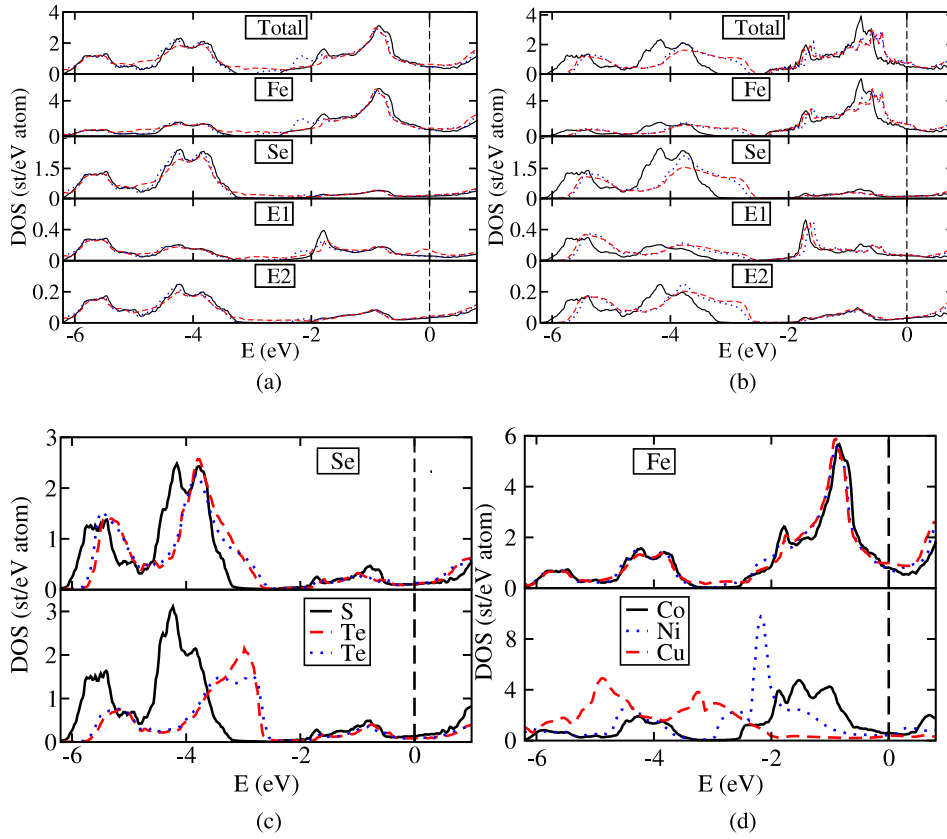
Figure 13. The total and the sub-lattice-resolved DOS of (a) S and Te substitutions on Se sub-lattice and (b) Co, Ni and Cu substitutions on Fe sub-lattice. The DOS in (a) correspond to $FeSe_{0.9}S_{0.1}$ (black, solid), $FeSe_{0.75}Te_{0.25}$ (blue, dotted) and $FeSe_{0.5}Te_{0.5}$ (red, dashed), and in (b) $Fe_{0.9}Co_{0.1}Se$ (black, solid), $Fe_{0.9}Ni_{0.1}Se$ (blue, dotted) and $Fe_{0.91}Cu_{0.1}Se$ (red, dashed). The vertical, dashed line denotes the Fermi energy. The atom-resolved, DOS of S and Te substitutions at the Se sub-lattice and Co, Ni and Cu substitutions at the Fe sub-lattice are shown in (c) and (d), respectively.
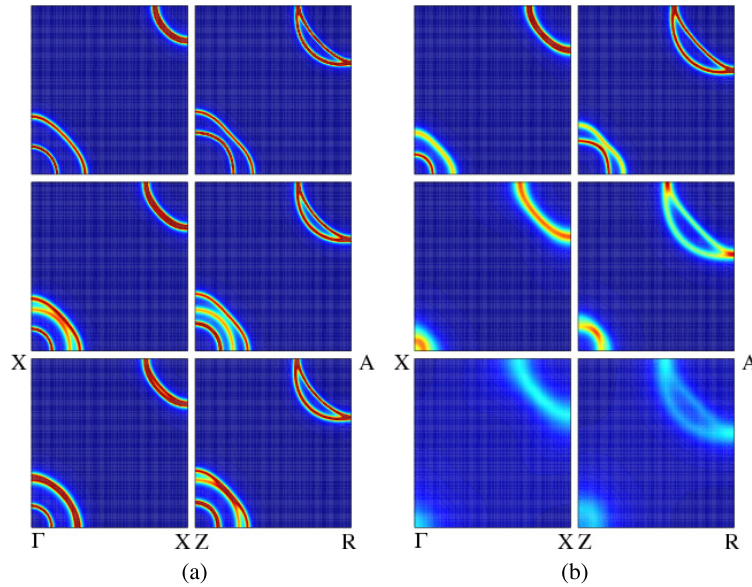

Figure 14. The Fermi surface of (a) $FeSe_{0.9}S_{0.1}$ (top), $FeSe_{0.75}Te_{0.25}$ (middle) and $FeSe_{0.5}Te_{0.5}$ (bottom), and (b) $Fe_{0.9}Co_{0.1}Se$ (top), $Fe_{0.9}Ni_{0.1}Se$ (middle) and $Fe_{0.91}Cu_{0.1}Se$ (bottom) in Γ–X–M and Z–R–A planes.

metals, in general, and in FeSe and its alloys, in particular, we have studied selected FeSe alloys using the rigid-band approximation, the virtual-crystal approximation and the supercell approximation. In this section, we describe and compare our results, in terms of DOS and Fermi surface, of the rigid-band approximation, the virtual-crystal approximation
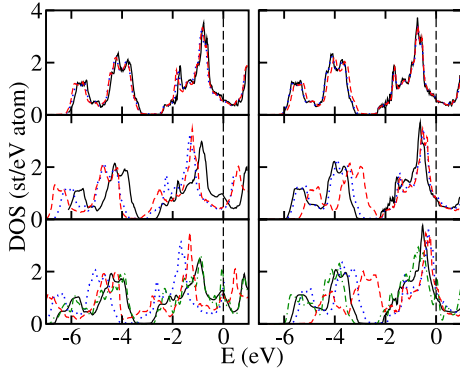
Figure 15. The total DOS of $Fe_{1+\delta}Se$ (left panel) and $FeSe_{1-x}$ (right panel) with δ and $x = 0.01$ (top), 0.06 (middle) and 0.125 (bottom) calculated in the rigid-band approximation (blue, dotted), the virtual-crystal approximation (red, dashed) and the coherent-potential approximation (black, solid). In the bottom panel, the total DOS obtained in the supercell approximation (green, double-dashed–dotted) using Fe_9Se_8 (left) and Fe_8Se_7 (right) are also shown. The vertical, dashed line denotes the Fermi energy.
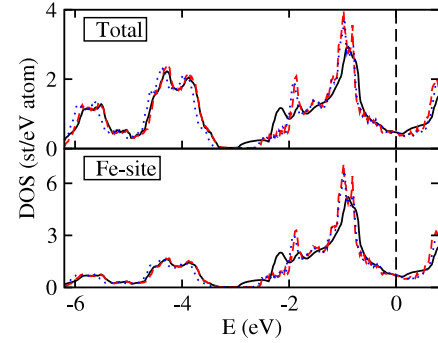

Figure 16. The total and the virtual-atom-site DOS of $Fe_{0.9}Ni_{0.1}Se$ (red, dashed), calculated in the virtual-crystal approximation as described in the text. The corresponding DOS in the rigid-band approximation (blue, dotted) and the coherent-potential approximation (black, solid) are also shown. The vertical, dashed line denotes the Fermi energy.

and the supercell approximation with that of the coherent-potential approximation for the selected FeSe alloys.

We have studied $Fe_{1+\delta}Se$ and $FeSe_{1-x}$ with δ and $x = 0.01, 0.06$ and 0.125, and $Fe_{0.9}Ni_{0.1}Se$ alloys in both the rigid-band approximation and the virtual-crystal approximation. For δ and $x = 0.125$, studied for comparison with the supercell approximation, we have used the lattice parameters corresponding to $\delta = 0.06$ and $x = 0.12$, respectively. We have also studied Fe_9Se_8 and Fe_8Se_7 as well as Fe_8Se_8 in the supercell approximation. The selected alloys cover a wide range of systems with effects due to disorder involving addition of d electrons in $Fe_{1+\delta}Se$, removal of s and p electrons in $FeSe_{1-x}$ and similar atoms in $Fe_{0.9}Ni_{0.1}Se$. Generally, one expects the rigid-band approximation to work well for free-electron-like systems or systems consisting of similar atoms. On the other hand, the virtual-crystal approximation is expected to work well for systems consisting of atoms from nearby columns of the periodic table such as $Fe_{0.9}Ni_{0.1}Se$. The supercell approximation or its more efficient version known as the special quasi-random structure [36] for describing the disordered alloy can be used to extract many properties of alloys such as the density of states and phase stability.

In figure 15, we compare the total DOS of $Fe_{1+\delta}Se$ and $FeSe_{1-x}$ with δ and $x = 0.01, 0.06$ and 0.125 calculated in the rigid-band and virtual-crystal approximations with that of the coherent-potential approximation. For δ and $x = 0.01$, we find that the total DOS obtained in the rigid-band approximation is close to that of the coherent-potential approximation. For higher concentrations, the rigid-band DOS begins to differ substantially from the CPA DOS for $Fe_{1+\delta}Se$. Not surprisingly, in $FeSe_{1-x}$ the Se vacancy, involving the absence of s and p electrons, leads to a relatively small disagreement up to $x = 0.06$.

For both $Fe_{1+\delta}Se$ and $FeSe_{1-x}$, the DOS calculated with the virtual-crystal approximation differs substantially with the CPA DOS for δ and $x \geqslant 0.06$, as can be seen from figure 15. Note that, for $x = 0.125$, the virtual-crystal

approximation replaces the Se atom on the Se sub-lattice in $FeSe_{1-x}$ by a virtual atom with atomic number equal to 33.25. Thus, we find that the virtual-crystal approximation essentially fails to describe accurately the effects of disorder in the DOS of either $Fe_{1+\delta}Se$ or $FeSe_{1-x}$ for δ and $x \geqslant 0.06$. However, the virtual-crystal approximation is expected to work better if the virtual atom is made out of atoms with similar atomic numbers, as in $Fe_{0.9}Ni_{0.1}Se$. In figure 16, we compare the total and the Fe sub-lattice DOS in $Fe_{0.9}Ni_{0.1}Se$ in the virtual-crystal approximation with the corresponding CPA DOS. Indeed, we find a good agreement in the DOS of $Fe_{0.9}Ni_{0.1}Se$. Some of the differences in the DOS of $Fe_{0.9}Ni_{0.1}Se$ around -1.9 and -1.0 eV highlight one of the shortcomings of the virtual-crystal approximation (as well as that of the supercell approximation) in assuming a periodic lattice with no energy-dependent electron scattering. The virtual-crystal approximation, as implemented here, cannot be applied to $FeSe_{0.5}Te_{0.5}$. A more appropriate approach for implementing the virtual-crystal approximation in alloys may be through the use of pseudopotentials [37].

In figure 15, the total DOS obtained for Fe_9Se_8 and Fe_8Se_7, corresponding to the supercell approximation for 0.125 of excess Fe and 0.125 of Se vacancy per atom in FeSe, respectively, are also shown. The total DOS for Fe_9Se_8 is in overall agreement with the corresponding CPA DOS of $Fe_{1.125}Se$. For the Se vacancy, the total DOS of Fe_8Se_7 is very close to the fully relaxed, full-potential supercell result of [23], as shown in their figure 2. A comparison of the supercell DOS of Fe_8Se_7 with the CPA DOS of $FeSe_{0.875}$ shows some differences around the Se region and around E_F. In particular, the sharp peak close to E_F is missing in the CPA DOS. If the presence of the peak is confirmed by experiment, then it would indicate the need to go beyond the single-site CPA. The supercell approximation does provide the possibility of including several atomic environments: however, its inherent flaw of not including energy-dependent electron scattering limits its applicability.

The **k**-resolved properties of alloys provide a more stringent test for the accuracy and the reliability of the various approximations for describing disorder that we have discussed
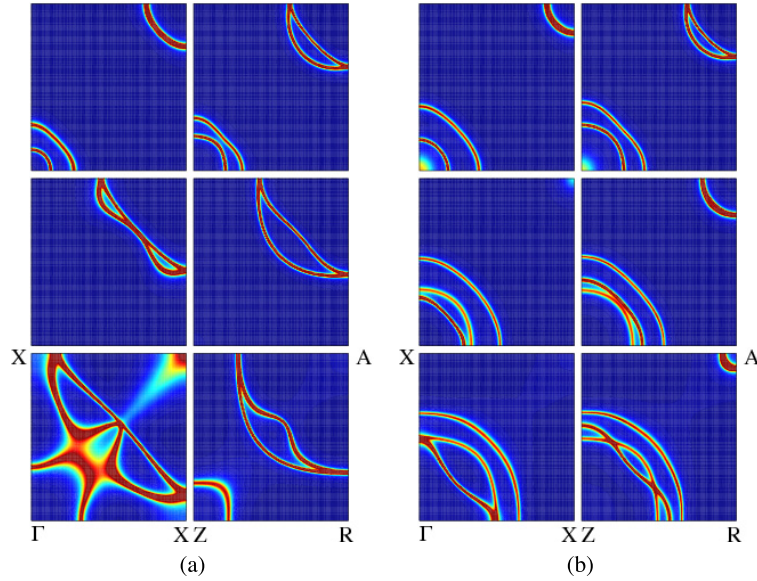
Figure 17. The Fermi surface, calculated in the rigid-band approximation as described in the text, of (a) $Fe_{1+\delta}Se$ and (b) $FeSe_{1-x}$ with δ and $x = 0.01$ (top), 0.06 (middle) and 0.125 (bottom) in Γ–X–M and Z–R–A planes.

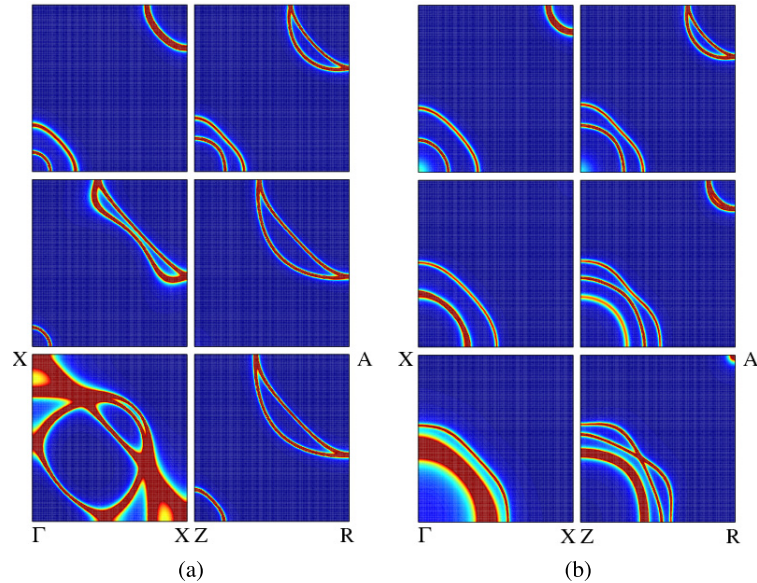**Figure 18.** The Fermi surface, calculated in the virtual-crystal approximation as described in the text, of (a) $Fe_{1+\delta}Se$ and (b) $FeSe_{1-x}$ with δ and $x = 0.01$ (top), 0.06 (middle) and 0.125 (bottom) in Γ–X–M and Z–R–A planes.

so far. Therefore, we have calculated the Fermi surface of the selected alloys in the Γ–X–M and Z–R–A planes in the rigid-band, virtual-crystal and supercell approximations, and the results are shown in figures 17–19. The Fermi surface of $Fe_{1+\delta}Se$ and $FeSe_{1-x}$ obtained in the rigid-band approximation, figure 17, agrees with the corresponding CPA Fermi surface, figure 10, for δ and $x = 0.01$ only. The Fermi surface obtained in the virtual-crystal approximation, shown in figure 18, disagrees with both the rigid-band, figure 17, and the CPA, figure 10, results for δ and $x \geqslant 0.06$. Similarly, for $Fe_{0.9}Ni_{0.1}Se$ the Fermi surface in the rigid-band approximation is closer to the corresponding CPA Fermi surface than the Fermi surface obtained in the virtual-crystal approximation as shown in figure 19(a). Finally, we show the Fermi surface

of Fe_8Se_8, Fe_9Se_8 and Fe_8Se_7 in figure 19(b), obtained in the supercell approximation. Due to the folding in k_x and k_y directions, the Fermi surface of Fe_9Se_8 and Fe_8Se_7 cannot be compared directly with the CPA Fermi surface obtained using the primitive cell. Therefore, we also show in figure 19(b) the Fermi surface of Fe_8Se_8. We find that the supercell approximation of Fe_9Se_8 and Fe_8Se_7 predicts a very different Fermi surface of disordered FeSe alloys than the coherent-potential approximation.

9. Conclusions

In conclusion, we have studied the electronic structure of $Fe_{1+\delta}Se$, $FeSe_{1-x}$ and $FeSe_{1-y}Te_y$ as a function of δ, x and y as well as $FeSe_{0.9}S_{0.1}$, $Fe_{0.9}Co_{0.1}Se$, $Fe_{0.9}Ni_{0.1}Se$ and
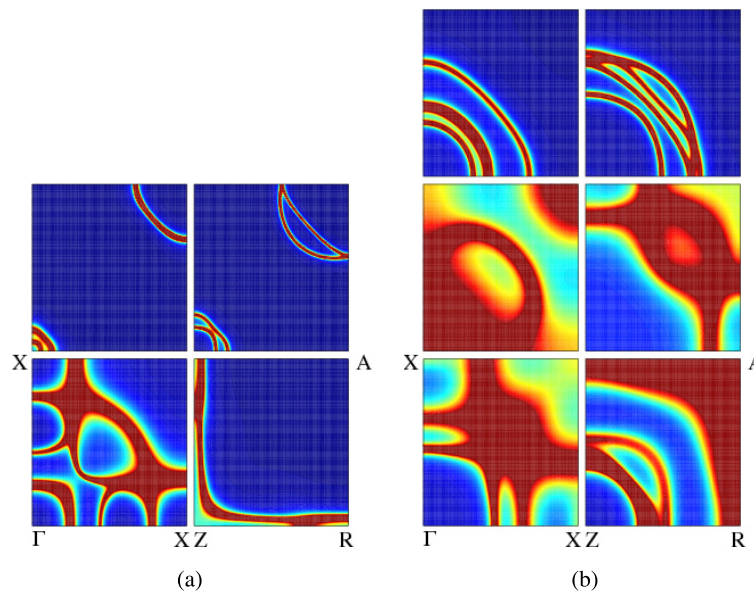
Figure 19. The Fermi surface of (a) $Fe_{0.9}Ni_{0.1}Se$, calculated in the rigid-band approximation (top) and the virtual-crystal approximation (bottom) in Γ–X–M and Z–R–A planes. In (b) the Fermi surfaces of Fe_8Se_8 (top), Fe_9Se_8 (middle) and Fe_8Se_7 (bottom) in Γ–X–M and Z–R–A planes, calculated using the supercell approximation, are shown.

$Fe_{0.91}Cu_{0.1}Se$ alloys. our results show that (i) a small amount of excess Fe substantially disorders the Fe-derived bands near E_F while the Se deficiency affects mainly the Se-derived bands away from E_F, (ii) the substitution of S and Te enhances the possibility of FS nesting in spite of disordering the Se-derived bands, especially in the $FeSe_{0.5}Te_{0.5}$ alloy and (iii) the substitution of Co, Ni or Cu disorders and pushes down the Fe-derived bands, thereby destroying the possibility of FS nesting. We also find that the coherent-potential approximation is more reliable than the rigid-band, virtual-crystal or supercell approximations for describing substitutional disorder in FeSe alloys. Thus, within the framework of spin-fluctuation theories, our results provide a consistent basis for understanding the superconducting properties of FeSe alloys.

Acknowledgment

References

[1] Kamihara Y, Watanabe T, Hirano M and Hosono H 2008 *J. Am. Chem. Soc.* **130** 3296
[2] Ren Z-A *et al* 2008 *Chin. Phys. Lett.* **25** 2215
[3] Hsu F-C, Luo J-Y, Yeh K-W, Chen T-K, Huang T-W, Wu P M and Lee Y-C 2008 *Proc. Natl Acad. Sci. USA* **105** 14262
[4] Drew A J *et al* 2008 *Phys. Rev. Lett.* **101** 097010
[5] Bao W *et al* 2009 *Phys. Rev. Lett.* **102** 247001
[6] Han M J, Yin Q, Pickett W E and Savrasov S Y 2009 *Phys. Rev. Lett.* **102** 107003
[7] Berk N F and Schrieffer J R 1966 *Phys. Rev. Lett.* **17** 433
[8] Monthoux P, Pines D and Lonzarich G G 2007 *Nature* **450** 1177
[9] Moriya T, Takahashi T and Ueda K 1990 *J. Phys. Soc. Japan* **59** 2905
[10] Moriya T 1985 *Spin Fluctuations in Itinerant Magnetism* (Berlin: Springer)
[11] Ishida K, Nakai Y and Hosono H 2009 *J. Phys. Soc. Japan* **78** 062001
[12] Mazin I I and Schmalian J 2009 arXiv:0901.4790
[13] Subedi A, Zhang L, Singh D J and Du M H 2008 *Phys. Rev.* B **78** 134514
[14] Mazin I I, Singh D J, Johannes M D and Du M H 2008 *Phys. Rev. Lett.* **101** 057003
[15] Mizuguchi Y, Tomioka F, Tsuda S, Yamaguchi T and Takano Y 2009 *J. Phys. Soc. Japan* **78** 074712
[16] McQueen T M, Williams A J, Stephens P W, Tao J, Zhu Y, Ksenofontov V, Casper F, Felser C and Cava R J 2009 *Phys. Rev. Lett.* **103** 057002
[17] Williams A J, McQueen T M and Cava R J 2009 *Solid State Commun.* **149** 1507–9
[18] McQueen T M *et al* 2009 *Phys. Rev.* B **79** 014522
[19] Mizuguchi Y, Tomioka F, Tsuda S, Yamaguchi T and Takano Y 2008 *Appl. Phys. Lett.* **93** 152505
[20] Margadonna S, Takabayashi Y, Ohishi Y, Mizuguchi Y, Takano Y, Kagayama T, Nakagawa T, Takata M and Prassides K 2009 arXiv:0903.2204
[21] Medvedev S *et al* 2009 *Nat. Mater.* **8** 630
[22] Yaresko A N, Liu G Q, Antonov V N and Andersen O K 2009 *Phys. Rev.* B **79** 144421
[23] Lee K W, Pardo V and Pickett W E 2008 *Phys. Rev.* B **78** 174502
[24] Zhang L, Singh D J and Du M H 2009 *Phys. Rev.* B **79** 012506
[25] Xu G, Ming W, Yao Y, Dai X, Zhang S-C and Fang Z 2008 *Eur. Phys. Lett.* **82** 67002
[26] Yu S-L, Kang J and Li J-X 2009 *Phys. Rev.* B **79** 064517
[27] Faulkner J S 1982 *Prog. Mater. Sci.* **27** 1
[28] Singh P P and Gonis A 1994 *Phys. Rev.* B **49** 1642
[29] Soven P 1967 *Phys. Rev.* **156** 809
[30] von Barth U and Hedin L 1972 *J. Phys. C: Solid State Phys.* **5** 1629
[31] Kubler J 1980 *J. Magn. Magn. Mater.* **15–18** 859
[32] Yin Z P, Lebegue S, Han M J, Neal B, Savrasov S Y and Pickett W E 2008 *Phys. Rev. Lett.* **101** 047001
[33] Perdew J P, Burke K and Ernzerhof M 1996 *Phys. Rev. Lett.* **77** 3865
[34] Perdew J P and Wang Y 1992 *Phys. Rev.* B **45** 13244
[35] Pomjakushina E, Conder K, Pomjakushina V, Bendele M and Khasanov R 2009 arXiv:0905.2115
[36] Zunger A, Wei S-H, Ferreira L G and Bernard J E 1990 *Phys. Rev. Lett.* **65** 353
[37] Bellaiche L and Vanderbilt D 2000 *Phys. Rev.* B **61** 7877